IEEE Photonics Journal
An IEEE Photonics Society Publication

Open Access

Low-Complexity TOAD-Based All-Optical Sampling Gate With Ultralow Switching Energy and High Linearity

Volume 7, Number 4, August 2015

P. Li
L. Jiang
J. G. Zhang
J. Z. Zhang
Y. C. Wang

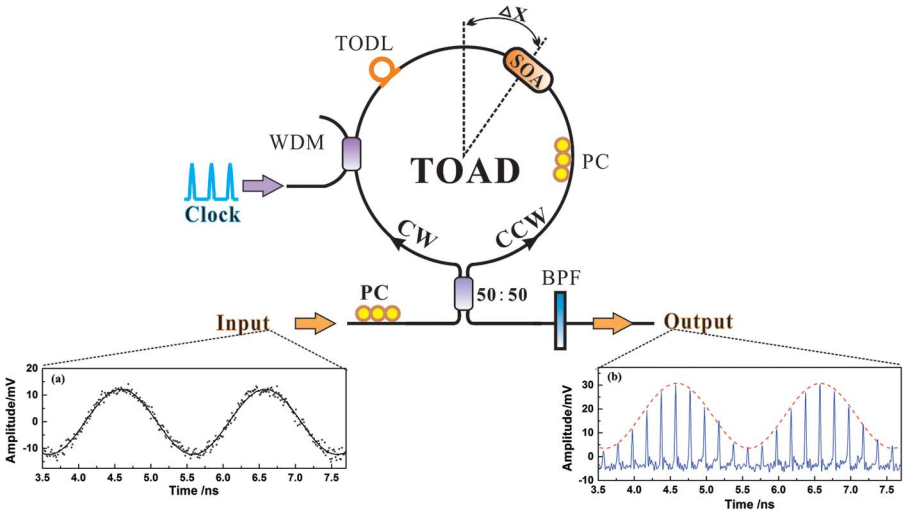

DOI: 10.1109/JPHOT.2015.2459377
1943-0655 © 2015 IEEE

IEEE photonics SOCIETY

IEEE

Low-Complexity TOAD-Based All-Optical Sampling Gate With Ultralow Switching Energy and High Linearity

P. Li,[1,2] L. Jiang,[1,2] J. G. Zhang,[1,2] J. Z. Zhang,[1,2] and Y. C. Wang[1,2]

[1]Key Laboratory of Advanced Transducers and Intelligent Control System, Ministry of Education and Shanxi Province, Taiyuan 030024, China
[2]Institute of Optoelectronic Engineering, College of Physics and Optoelectronics, Taiyuan University of Technology, Taiyuan 030024, China

DOI: 10.1109/JPHOT.2015.2459377

Manuscript received May 31, 2015; revised July 2, 2015; accepted July 17, 2015. Date of publication July 21, 2015; date of current version July 30, 2015. This work was supported in part by the National Natural Science Foundation of China under Grant 61227016, Grant 61205142, and Grant 51404165; and in part by Shanxi Natural Science Foundation of China under Grant 2015021088. Corresponding author: Y. C. Wang (e-mail: wangyc@tyut.edu.cn).

Abstract: We present experimentally a low-complexity ultralow switching energy and high-linearity all-optical sampling gate based on a terahertz optical asymmetric demultiplexer, constructed by placing a polarization-insensitive multiple-quantum-well semiconductor optical amplifier (PI-MQW-SOA) asymmetrically within a fiber loop mirror. Using a picosecond pulse train as the trigger clock, we analyze, in detail, the influence of the sampling pulse power and the offset of the PI-MQW-SOA from the loop midpoint on the shape, width, and amplitude of the sampling window, respectively. Furthermore, the switching energy and linearity of this sampling gate under different widths of sampling windows are specifically investigated. Results demonstrate that our sampling gate possesses a switching energy as low as 25 fJ and a high linearity above 0.99.

Index Terms: All-optical sampling, semiconductor optical amplifier, optical signal processing.

1. Introduction

The all-optical sampling gate is the core of a sampling system. Low switching energy and high linearity are two critical factors to access the performance of an all-optical sampling gate [1]. The requirement of low energy cannot only reduce the power consumption of the device, but importantly also effectively reduce the system complexity due to the absence of any booster amplifiers. The factor of linearity directly reflects the signal distortion after sampling. The higher the linearity is, the less the distortion. Moreover, the low-complexity is another key factor from the view of practical applications, which requires the all-optical sampling gate must be in a small enough size and has the ability to be integrated.

Generally, all-optical sampling gates are achieved by means of optical nonlinearity in some mediums. In early researches, crystals are the most widely used nonlinear mediums. There have been many reports about sampling gates based on second-order optical nonlinearity in crystals such as KTP [2], [3], AANP [4], and PPLN [5], [6] since Duguay *et al.* implemented all-optical sampling by utilizing sum frequency generation (SFG) in a KDP crystal in 1968 [7]. However, this

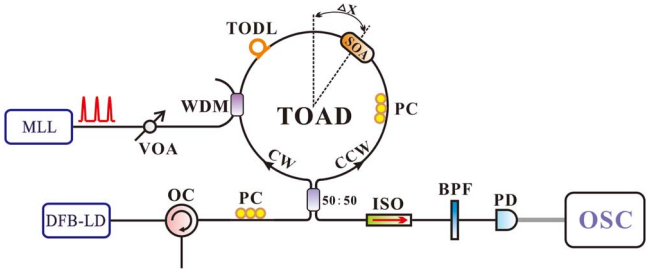

Fig. 1. Experimental setup of the proposed all-optical sampling gate. MLL: mode-locked laser; VOA: variable optical attenuator; WDM: wavelength division multiplexer coupler; TODL: tunable optical delay line; SOA: semiconductor optical amplifier; PC: polarization controller; DFB-LD: distributed feedback laser diode; OC: optical circulator; 50:50, 50:50 coupler; ISO: optical isolator; BPF: optical band-pass filter; PD: photoelectric detector; OSC: oscilloscope; CW and CCW: clockwise and a counterclockwise propagating signal; TOAD: terahertz optical asymmetric demultiplexer.

kind of technique requires the sampling clock energy be of several hundred pJ. Until 1991, Andrekson *et al.* succeeded in achieving an all-optical sampling configuration by employing four wave mixing (FWM) in a 14 km fiber [8]. Thenceforth optical fibers attracted serious concern as another nonlinear material. Especially with the appearance of highly nonlinear optical fibers (HNLF), many different nonlinear effects such as FWM [9], [10], optical parametric amplification (OPA) [11], [12], cross-phase modulation (XPM) [13]–[15] have been used to implement optical sampling functions. Nevertheless, the long interaction lengths required for sampling in nonlinear fibers (typically kilometers) make these fiber-based schemes extremely complex and sensitive to environmental fluctuations and limit these techniques to specialized applications.

Recently, semiconductor optical amplifiers (SOAs) begin to receive attention as a novel all-optical sampling element, due to its compact size and large nonlinearity coefficient. Several sampling schemes have been proposed by exploiting FWM [16]–[18], XPM [19]–[21] and nonlinear polarization rotation (NPR) [22] in SOAs, respectively. Among them, all-optical sampling gates based on the terahertz optical asymmetric demultiplexer (TOAD) are very attractive because of its simplicity, stability and ease to integration [20], [21]. A very spectacular result in terms of energy is implemented by Bogoni *et al.*, where the energy of sampling clock pulse is about 320 fJ [21]. However, that still is somewhat energy-wise expensive in actual operation. At the same time, it should be mentioned that there has been no investigation about the effect of the associated parameters on the sampling performance in all these reports on TOAD-based sampling gates.

In this letter, we employ a polarization-insensitive multiple quantum well semiconductor optical amplifier (PI-MQW-SOA) as the nonlinear element and implement experimentally a TOAD-based sampling gate with ultra-low switching energy and high linearity. We analyze in detail the influence of the sampling pulse power and the asymmetrical offset of the SOA on the shape, width and amplitude of the sampling window, respectively. Further, the switching energy and linearity of this sampling gate are in particularly investigated under different width of sampling windows. Experimental results show that our sampling gate possesses a switching energy as low as 25 fJ and a high linearity above 0.99, indicating a high sampling fidelity. To the best of our knowledge, this is the lowest energy sampling gate based on TOAD so far.

2. Experimental Setup

Fig. 1 is the proposed all-optical sampling gate based on the architecture of TOAD. It is a Sagnac interferometer consisting of a loop mirror with additional intra-loop elements: a 50:50 coupler (50:50), a wavelength division multiplexer coupler (WDM), a tunable optical delay line (TODL), a polarization controller (PC), and a PI-MQW-SOA (SOA) as the nonlinear medium. The PC placed in the loop is used to adjust the polarization to maximize the on-off ratio of the

interferometer, while the SOA is offset from the loop midpoint by a distance Δx, which can be precisely controlled via the TODL.

Through a variable optical attenuator (VOA), a train of clock pulses generated from an ultrafast mode-locked laser (MLL) as the sampling signal are coupled into the loop via the WDM. At the same time, a continuous-wave signal generated from a DFB laser diode (DFB-LD) to be sampled enters the loop via the 50:50 coupler through an optical circulator (OC) and splits into two signals: a clockwise (CW) and a counterclockwise (CCW) propagating signal. The clock pulse saturates the SOA so that the CW and CCW signal components experience a different phase modulation when they pass through the device before and after the clock pulse, respectively. Otherwise, they are affected by the same phase modulation. These two conditions allow us to obtain two different transmission values and, thus, form a sampling window with a time length Δt[$\Delta t = 2\Delta x/v_g$, where v_g represents the group-velocity of the CW and CCW signal in the loop]. The sampling window is opened periodically with the arrival of clock pulse, so the input waveform can be sampled at the repetition rate of the clock. Finally, with optical band-pass filter (BPF), we can separate the sampled output from the optical clock and ASE noise because their operating wavelengths are different, and then visualize it on a digital real-time oscilloscope (OSC) via a photoelectric detector (PD). Note, the optical isolator (ISO) close to the output port of the TOAD is required to prevent the back flow of the reflected signal and sampling clock.

In the experiment, the Gaussian pulse train from the MLL (Pritel, UOC-05-14G-E) as the sampling clock operates at a wavelength of 1551 nm, which has a full width at half maximum (FWHM) of 2.2 ps, a repetition rate of 5 GHz and a timing jitter smaller than 50 fs. By adjusting the VOA, we can changes the average power of sampling pulse from -16 dBm to -4 dBm. The continuous wave generated by the DFB-LD (WTD, LDM5S752) works at a wavelength of 1553 nm. The CW and CCW signal have almost the same average power about 56 μW. The SOA (Kamelian, SOA-NL-L1-C-FA) is a 1000 μm PI-MQW nonlinear SOA biased at 300 mA, operating at a peak gain wavelength of 1550 nm with a small-signal gain of 26 dB and having a 3-dB bandwidth of 64 nm and a gain recovery time of 25 ps. The BPF works at a center wavelength of 1553 nm with a 3-dB bandwidth of 0.2 nm. The bandwidth of the PD (U2T, XPDV2120RA) and OSC (Lecroy, LabMaster10-36Zi) is 40 GHz and 36 GHz, respectively.

3. Experimental Results

We first analyze the effect of two important parameters to the sampling window, i.e., the clock pulse power and the SOA asymmetric offset, before demonstrating the ultra-low switching energy and high linearity of the all-optical sampling gate.

3.1. Effects of the Clock Pulse on the Sampling Window

In our system, the clock power governs the experienced differential phase shift between the CW and CCW signal components, which determine the final output level of the sampling gate. Fig. 2(a) shows a set of sampling window shapes under different average power of clock pulses varied from -16 to -4 dBm in a step of 0.5 dBm, while the offset time–length Δt is fixed at about 30 ps. Each condition has two sampling windows whose time interval is 200 ps, just corresponding to the repetition of the clock. It can be seen qualitatively the power of clock pulse have a significant effect on the amplitude of window and there exists an optimal sampling power, but nearly no effect on the size of windows along the x-axis. In order to display this feature more directly, we extract some windows and show them in Fig. 2(b). Obviously, the window amplitude increases firstly and then reduces with the increase of the sampling pulse power. However, these window sizes keep the same as each other because they are determined by the asymmetrical offset. Here, the window size is a time width of window, quantitatively defined as the transmission window width where the amplitude is above 0 mV [see the dashed line in Fig. 2(b)]. Fig. 2(c) is the evolution of the normalized window amplitude versus different average power clock. When the mean power of the sampling clock is -9 dBm, the window amplitude locates at the optimal

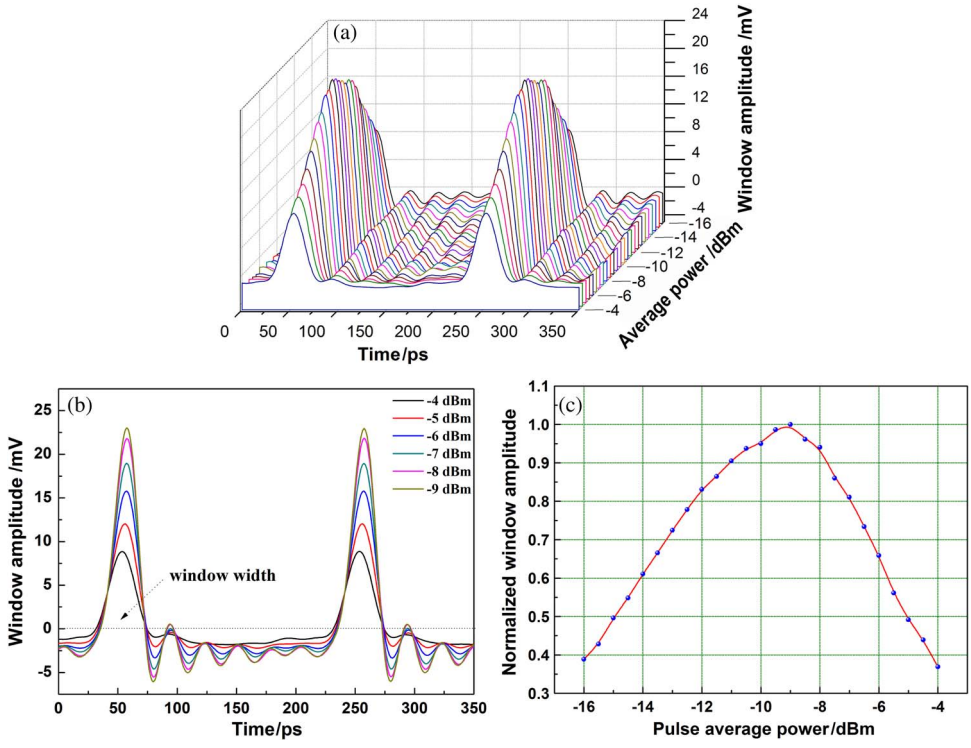

Fig. 2. Influence of sampling pulse power on the sampling window. (a) Shape, (b) width, and (c) normalized amplitude of the sampling window. The dashed line denotes 0 mV.

value, indicating that the output signal level is the highest at this point. The reason why the window amplitude has a maximum and for high power the window amplitude starts to decrease can be explained as below: the phase shift $\Delta\varphi$ caused by the sampling pulse will take on a monotone increasing from 0 to 2π with the increase of the sampling pulse power. The window amplitude P_{out} roughly satisfies $P_{out} \propto P_{in}\left[G_{CW} + G_{CCW} - 2 \bullet (G_{CW} \bullet G_{CCW})^{1/2} \bullet \cos(\Delta\varphi)\right]$, where P_{in} represents the power of the continuous-wave signal generated from the DFB-LD to be sampled, G_{CW} and G_{CCW} denote the gains which CW and CCW signal achieved through the SOA, respectively. Only when the phase shift $\Delta\varphi$ experienced by CW and CCW equals does, the constructive interference occur, and thus, the amplitude will arrive the highest value which corresponds to the optimal power in Fig. 2(b). Otherwise, the associated amplitude will decreases no matter when the sampling pulse power is stronger or weaker than the optimal power. Note, the weak oscillation structure behind every sampling window is caused "ringing phenomenon" from imperfect impedance matching between the PD and electrical cable used for observing.

3.2. Effect of the SOA Offset on the Sampling Window

The asymmetrical offset Δt is determined by adjusting the TODL in our experiment, which is determined by the distance by which the SOA is offset from the TOAD loop midpoint and unrelated with the clock jitter. Fig. 3(a) depicts sampling windows with extinction ratios of 20 dB under different offsets increased from 2 to 20 ps with a step of 1 ps, while the average power of sampling clock pulse is -9 dBm. Through decreasing the SOA offset, one can reach smaller windows at the expense of having reduced extinction ratios. Like Fig. 2(a), each asymmetry in Fig. 3(a) corresponds to two sampling windows whose time interval just corresponds to the repetition of the clock. However, the difference is that the asymmetry not only has a significant influence on the amplitude of window but determines the width of windows as well. In order to display these characteristics more clearly, we extract several windows corresponding to these

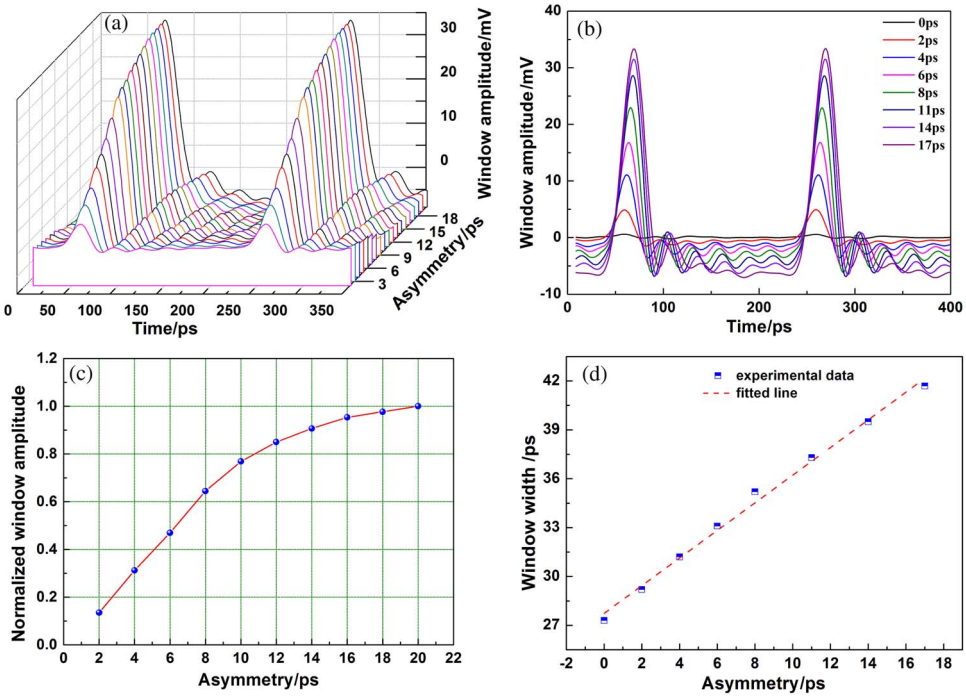

Fig. 3. Influence of the SOA asymmetric offset on the sampling window. (a) Shape, (b) width, (c) normalized amplitude of the sampling window, and (d) window width as function of asymmetry.

asymmetry from 2 ps to 17 ps, respectively. As shown in Fig. 3(b), both the window amplitude and width decrease since the associated asymmetry is reduced. Note, these sampling windows have approximately overlapped rise edge, although their width is different. That is because the rise edge is determined by the intrinsic rise-time of the nonlinearity in SOA, which is associated with sampling pulse width directly. These features are consistent with theoretical results in [23]. Fig. 3(c) shows the dependence of normalized window amplitude on the asymmetry: the normalized amplitude enhances sharply at first and then gradually converges to a stable value with the increase of the asymmetry. Fig. 3(d) is a plot of window width as function of asymmetry. The minimum temporal resolution of the present scheme is about 27 ps, where the time offset of the SOA is 0 ps, as shown in Fig. 2(b) and (d). This resolution is limited by the SOA length.

3.3. Performance Evaluation of the Sampling Gate

Now, we make the performance evaluation to the sampling gate. The low switching energy and high linearity are the two critical factors to access the performance of an all-optical sampling gate, as explained in the Introduction.

The switching energy represents the optimal energy of sampling clock pulse which just induces a π phase difference between the CW and CCW signal, when the width of sampling window is fixed through precisely fixed the length of the TODL. From the point view of the final output level of our sampling gate, the switching energy corresponds to the energy of clock pulse where the amplitude of sampling window is the maximum. Fig. 4(a) shows the evolution of the sampling window amplitude with the increase of clock pulse power under different window widths. It is clear that there exists an optimal power of sampling pulse at each window width. Moreover, these optimal power values are the same as each other, where the window amplitude corresponds to the maximum. Fig. 4(b) shows the switching energy under different sampling window widths in detail. These widow widths have nearly no effect on the switching energy and they approximately remains at an average energy of 24 fJ with a weak fluctuation in the

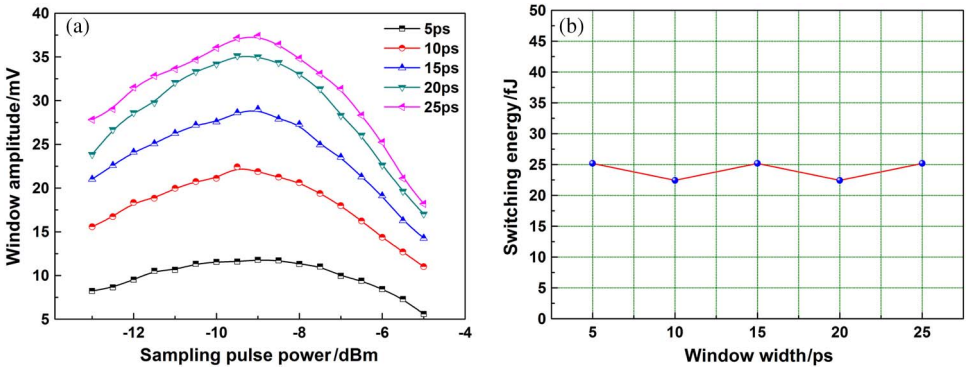

Fig. 4. (a) Dependence of the window amplitude on the power of sampling pulse under different window widths. (b) Switching energy under different window widths.

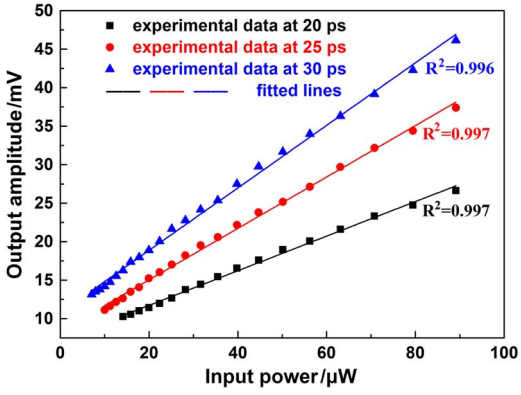

Fig. 5. Linearity of the TOAD-based gate. Dependence of output signal power on input signal power under different sampling window widths at the asymmetries: 30 ps, 25 ps, and 20 ps. Note that the solid mark is experimental data, the line is the fitted curve, and R2 represents the associated linearity.

range of ± 1 fJ. The switching energy corresponds to the optimal sampling pulse power, the highest point in Fig. 4(a). After determining the optimal sampling pulse power from Fig. 4(a), we can calculate the switching energy according to the widely applied formula: Switching Energy [J] = Sampling Pulse Power [W] $\times$ Sampling Period [s]. For example, when the sampling pulse power is about -9 dBm and the sampling period is 200 ps, respectively, so the switching energy can be calculated and equals to a value about 25 fJ.

The linearity indicates how the sampling fidelity is. Ideally, the linearity should be 1 for a perfect all-optical sampling gate. Fig. 5 is the relationship between the amplitude of the sampled output signal and the power of input signal to be sampled under different sampling window widths in our system. Those solid points and lines in Fig. 5(a)–(c) represent experimentally measured data and associated fitted lines, respectively. Herein, we just take the sampling window widths at the asymmetries of 30 ps, 25 ps and 20 ps as examples. It can be seen that a linear dependence of the amplitude of the sampled output signal on the input signal power over a dynamic range about 20 dB. Quantitatively, all linearity of R^2 under different window widths is more than 0.99.

Further, we give a more intuitive evidence to demonstrate the good performance of our sampling gate through the famous visual sine wave test. In this test, the signal to be sampled in Fig. 1 is replaced by a 500 MHz sine optical signal with an average power of 10 μW which is generated by modulating an electrical sine wave into the 1553 nm stable continuous-wave source via an 20 GHz electro-optic modulator (EOSPACE, AZ-DK5-20-PKU-SFU-LV-SRF1W).

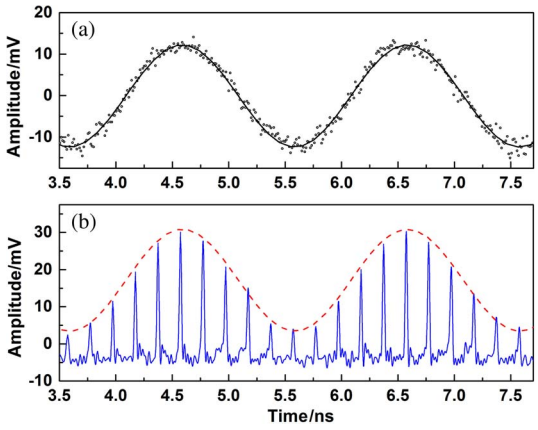

Fig. 6. Visual sine wave test on the proposed all-optical sampling gate. (a) 500-MHz sine optical wave to be sampled recorded by the digital real-time OSC. (b) Output from the sampling gate. The dashed line is the waveform envelope of the sampled output peaks.

Fig. 6 shows a typical experimental test result. The sine waveform recorded directly by the 40 GHz PD and 36 GHz OSC is shown in Fig. 6(a). Fig. 6(b) is the associated sampled output optical pulse stream from the all-optical sampling gate when the sampling window width is fixed at the asymmetry of 30 ps. As it shown, the peak amplitude of the sampled output pulses are matched the sine wave very well, which directly indicates a high-fidelity sampling.

4. Conclusion

Using a polarization-insensitive multiple quantum well semiconductor optical amplifier (PI-MQW-SOA) as the nonlinear element, we demonstrated experimentally an ultra-low energy and high linearity TOAD-based all-optical sampling gate. The influence of the clock pulse power and the SOA asymmetrical offset Δx on the sampling window (including shape, amplitude, and width) gets analyzed in detail, respectively. Further, the switching energy and linearity of this sampling gate are in particularly investigated. The results indicate that our sampling gate combines a switching energy of 25 fJ and a high linearity above 0.99. Such a energy triggering clock and the potential to be integrated into a chip makes our scheme a more competitive alternative with respect to other correlated techniques.

Acknowledgements

The authors wish to thank the anonymous reviewers for their valuable suggestions.

References

[1] C. Schmidt-Langhorst and H. G. Weber, “Optical sampling techniques,” *J. Opt. Fiber Commun. Rep.*, vol. 2, no. 1, pp. 86–114, Mar. 2005.
[2] H. Takara, S. Kawanishi, T. Morioka, K. Mori, and M. Saruwatari, “100 Gbit/s optical waveform measurement with 0.6 ps resolution optical sampling using subpicosecond supercontinuum pulses,” *Electron. Lett.*, vol. 30, no. 14, pp. 1152–1153, 1994.
[3] H. Takara, S. Kawanishi, and M. Saruwatari, “Optical signal eye diagram measurement with subpicosecond resolution using optical sampling,” *Electron. Lett.*, vol. 32, no. 15, pp. 1399–1400, Jul. 1996.
[4] H. Takara *et al.,* “100 Gbit/s optical signal eye-diagram measurement with optical sampling using organic nonlinear optical crystal,” *Electron. Lett.*, vol. 32, no. 24, pp. 2256–2258, Nov. 1996.
[5] S. Nogiwa, Y. Kawaguchi, H. Ohta, and Y. Endo, “Highly sensitive and time-resolving optical sampling system using thin PPLN crystal,” *Electron. Lett.*, vol. 36, no. 20, pp. 1727–1728, Sep. 2000.
[6] S. Nogiwa, H. Ohta, Y. Kawaguchi, and Y. Endo, “Improvement of sensitivity in optical sampling system,” *Electron. Lett.*, vol. 35, no. 11, pp. 917–918, May 1999.
[7] M. A. Duguay and J. W. Hansen, “Optical sampling of subnanosecond light pulses,” *Appl. Phys. Lett.*, vol. 13, no. 5, pp. 178–180, 1968.

[8] P. A. Andrekson, "Picosecond optical sampling using four-wave mixing in fibre," *Electron. Lett.*, vol. 27, no. 16, pp. 1440–1441, Aug. 1991.
[9] M. Westlund, H. Sunnerud, B. Olsson, and P. A. Andrekson, "Simple scheme for polarization-independent all-optical sampling," *IEEE Photon. Technol. Lett.*, vol. 16, no. 9, pp. 2108–2110, Sep. 2004.
[10] S. I. Oda, A. Maruta, and K. Kitayama, "All-optical quantization scheme based on fiber nonlinearity," *IEEE Photon. Technol. Lett.*, vol. 16, no. 2, pp. 587–589, Feb. 2004.
[11] J. Li, J. Hansryd, P. O. Hedekvist, P. A. Andrekson, and S. N. Knudsenet, "300-Gb/s eye-diagram measurement by optical sampling using fiber-based parametric amplification," *IEEE Photon. Technol. Lett.*, vol. 13, no. 9, pp. 987–989, Sep. 2001.
[12] K. K. Y. Wong, M. E. Marhic, K. Uesaka, and L. G. Kazovsky, "Polarization-independent one-pump fiber-optical parametric amplifier," *IEEE Photon. Technol. Lett.*, vol. 14, no. 11, pp. 1506–1508, Nov. 2002.
[13] J. Li *et al.,* "0.5-Tb/s eye-diagram measurement by optical sampling using XPM-induced wavelength shifting in highly nonlinear fiber," *IEEE Photon. Technol. Lett.*, vol. 16, no. 2, pp. 566–568, Feb. 2004.
[14] A. Jolly and C. Granier, "All-optical sampling with Sagnac switches using closed pump and signal wavelengths near 1 μm," *Opt. Commun.*, vol. 281, no. 14, pp. 3861–3871, Jul. 2008.
[15] P. Li, Y. C. Wang, and J. Z. Zhang, "All-optical fast random number generator," *Opt. Exp.*, vol. 18, no. 19, pp. 20 360–20 369, Sep. 2010.
[16] S. Diez *et al.,* "Simultaneous sampling of optical pulse intensities and wavelengths by four-wave mixing in a semiconductor optical amplifier," *Appl. Phys. Lett.*, vol. 73, no. 26, pp. 3821–3823, 1998.
[17] S. Diez, R. Ludwig, C. Schmidt, U. Feiste, and H. G. Weber, "160-Gb/s optical sampling by gain-transparent four-wave mixing in a semiconductor optical amplifier," *IEEE Photon. Technol. Lett.*, vol. 11, no. 11, pp. 1402–1404, Nov. 1999.
[18] M. Shirane, Y. Hashimoto, H. Yamada, and H. Yokoyama, "A compact optical sampling measurement system using mode-locked laser-diode modules," *IEEE Photon. Technol. Lett.*, vol. 12, no. 11, pp. 1537–1539, Nov. 2000.
[19] S. Fischer *et al.,* "All-optical sampling with a monolithically integrated Mach–Zehnder interferometer gate," *Opt. Lett.*, vol. 26, no. 9, pp. 626–628, May 2001.
[20] K. L. Deng, R. J. Runser, I. Glesk, and P. R. Prucnal, "Single-shot optical sampling oscilloscope for ultrafast optical waveforms," *IEEE Photon. Technol. Lett.*, vol. 10, no. 3, pp. 397–399, Mar. 1998.
[21] A. Bogoni, F. Ponzini, M. Scaffardi, P. Ghelfi, and L. Potì, "New optical sampler based on TOAD and data postprocessing for subpicosecond pulse resolution," *IEEE J. Sel. Top. Quant.*, vol. 10, no. 1, pp. 186–191, Jan./Feb. 2004.
[22] I. Kang and K. F. Dreyer, "Sensitive 320 Gbit/s eye diagram measurements via optical sampling with semiconductor optical amplifier-ultrafast nonlinear interferometer," *Electron. Lett.*, vol. 39, no. 14, pp. 1081–1083, 2003.
[23] P. Toliver, R. J. Runser, I. Glesk, and P. R. Prucnal, "Comparison of three nonlinear interferometric optical switch geometries," *Opt. Commun.*, vol. 175, no. 4, pp. 365–373, Mar. 2000.